Development of a novel boring tool with anisotropic dynamic stiffness to avoid chatter vibration in cutting

Part 2: Analytical and experimental verification of the proposed method

Wataru Takahashi[1], Norikazu Suzuki[2], Eiji Shamoto[2]

Affiliations: [1] Mitsubishi Materials Corpration, 1-600 Kitabukuro-cho, Omiya-ku, Saitama-Shi, Saitama

[2] Nagoya University, Furo-cho, Chikusa-ku, Nagoya, 464-8603, Japan

In this study, we developed prototypes of boring tools with anisotropic dynamic stiffness, and their chatter stability was investigated analytically and experimentally. In Part 1, a novel design of boring tools with an anisotropic structure was proposed to improve the nominal stiffness in boring operation, thus resulting in higher chatter stability in simulation. In this part (Part 2), anisotropic boring tools with a holder length-to-diameter ratio (L/D) of 4 and 10 designed in Part 1 were prototyped, and their frequency response functions were evaluated. Then, the chatter stabilities were evaluated through turning experiments. With respect to a L/D4 boring tool with anisotropic structure, the nominal dynamic stiffness was significantly improved within the range of machining conditions that satisfies the appropriate combination of cutting force ratio and chip flow direction, compared to a conventional tool with isotropic structure. We confirmed that the proposed boring tool with an anisotropic structure increases the critical radial depth of cut by approximately 17 times compared with conventional tools. Even with an L/D10 anisotropic boring tool, a similar effect was observed wherein the dynamic stiffness of the tool was improved. In contrast, the effect of improving the dynamic stiffness was insufficient; thus, chatter free cutting could not be realized. Analytical investigations verified the importance of further improvement of dynamic characteristics. To realize stable boring with L/D10 boring tools, it is necessary to further reduce the system compliance while also improving the similarity of the frequency response function.

Key words: Cutting, Chatter, Boring, Dynamic stiffness, Anisotropy, Stability

1. Introduction

Boring operations using boring tools can create arbitrary hole diameters without relying on the tool diameter and can be used even for boring large diameter holes which may be difficult with drilling operations. Simultaneously, high-accuracy processing can be achieved. Thus, this method is often employed in production sites. However, boring operations have disadvantages in that the stiffness of the tool holder can easily deteriorate and chatter vibration can occur, which decreases the machining accuracy and tool life. Chatter vibration occurs because of interactions between the dynamic behavior of the mechanical structure and the cutting process, which accompanies the reproduction effects [1]. This phenomenon is particularly likely to occur when the structural stiffness of the machining system is low (e.g., in boring operations); this can be problematic because it significantly constrains the efficiency of the production process [2]. Therefore, many researchers have focused on the analysis and suppression of chatter vibration. Eynian et al. proposed a model for the turning process and an analysis method for its stability limit [3]. Shamoto et al. proposed a method to quantify the stability during boring operations using a gain margin [4]. These methods are also used in this study.

This research seeks to establish a novel anisotropy design which increases the chatter stability during boring operations. Anisotropic transfer characteristics are developed by applying a tapered horn and notch shape on the boring tool, and we attempt to make the dynamic stiffness during the boring process infinitely large. Reference [5] in Part 1 explained the basic design concept, and Part 1 [6] analytically clarified the effects that errors in the design of transfer characteristics have on the process stability performance. Analytical results showed that similarities between the diagonal components of the frequency response function (FRF) in the mode coordinate system were important and that the deterioration of similarity brought decreased the stability. The FRF needs to be adjusted so that the natural frequency and damping ratio match between vibration modes to improve similarity. Thus, a boring tool with an anisotropic structure that could achieve the desired dynamic characteristics was designed, and the FRF was estimated using FEM analysis. The results of FEM analysis showed that suitably designing an anisotropic structure can greatly improve the chatter stability relative to that in a general-use tool.

Thus, the proposed method may be able to effectively improve the functionality of the dynamic stiffness during the boring process. Investigations in Part 1 were based purely on simulations, and its applicability has not yet been verified with actual processes. Actual prototyped tools generate errors that cannot be

modeled, and these are thought to induce problems that deteriorate the expected chatter suppression effects. Thus, in Part 2, we fabricated prototypes of the tool holder designed in Part 1, verified the stability performance with hammering tests and boring operation experiments, and clarified the issues related to practical application.

In this paper, Section 2 outlines the analysis model for the chatter vibration stability limit during boring operations, Section 3 implements assessments of vibration characteristics in the prototyped tool, and Section 4 conducts verifications with experiments. Finally, the conclusions are presented.

2. Analysis model of chatter vibration stability limit during boring operation

The modeling of the boring process is explained in Part 1 [6]. A block diagram of the formulated boring process is shown in Fig. 1. This manuscript uses the following formulations based on the same model. The specific cutting force in the thrust direction during orthogonal cutting is denoted by K_t, and the ratio of the thrust force to the principal force is denoted by K_r. The projection width of the cutting edge contacting the workpiece along the feed direction is set as the cutting width b. Of this range contacting the cutting edge, the projection component in the feed direction of the contact width between the cutting edge and workpiece prior to a single rotation is set as the regenerative width b_d. These widths can be determined from the radial depth of cut d_r, feed per rotation c, and the tool shape. Furthermore, the rotational period of the work spindle is set as T, the chatter vibration frequency is set as ω_c, and the chip flow angle is set as η. As shown in the block diagram, the nominal FRF $\Phi(i\omega_c)$ in the boring process is obtained from Eq. (1) using the diagonal and off-diagonal components of the two-degree-of-freedom transfer function G_{xx} and G_{xy}. $\Phi(i\omega_c)$ is the one-degree-of-freedom transfer function that considers the chip flow angle η and force ratio K_r during the turning/boring process; it is defined as the equivalent transfer function in this research.

$$\Phi(i\omega_c) = \cos\eta\, G_{xx}(i\omega_c) + \frac{G_{xy}(i\omega_c)}{K_r} \qquad (1)$$

The equivalent transfer function $\Phi(i\omega_c)$ needs to satisfy Eq. (2) for the stability limit of the chatter vibration.

$$1 + K_t(b_d + c - b_d e^{-i\omega_c T})\Phi(i\omega_c) = 0 \qquad (2)$$

The stability limit of the system can be obtained by solving for the characteristic equation in this cutting

process. The equivalent transfer function $\Phi(i\omega_c)$ is the nominal stiffness that represents the system and is an important indicator for the assessment of stability.

Here, the stability corresponding to an arbitrary machining condition is quantitatively assessed by introducing the gain margin g_m and solving for Eq. (3).

$$1 + g_m K_t (b_d + c - b_d e^{-i\omega_c T})\Phi(i\omega_c) = 0 \qquad (3)$$

g_m is a positive real number, and the stability, instability, and stability limits are denoted as $g_m > 1$, $0 < g_m < 1$, and $g_m = 1$, respectively. Equation (3) can be modified in the following manner.

$$g_m = \frac{-1}{K_t(b_d + c - b_d e^{-i\omega_c T})\Phi(i\omega_c)} \qquad (4)$$

The value of g_m obtained from Eq. (4) is a complex number, and its imaginary part should be selected as the smallest and most unstable positive value among the real g_m parts $\mathrm{real}(g_m)$ which satisfy $\mathrm{imag}(\mathrm{g}_m) = 0$. If the workpiece is assumed to contact the circular arc range of the cutting edge, the regenerative width b_d can be determined from the following equation using the nose radius R of the tool.

$$b_d = \sqrt{2Rd_r - d_r^2} - \frac{c}{2} \qquad (5)$$

The chip flow angle η can be approximated with the following equation under the same assumptions.

$$\eta \approx \tan^{-1}\frac{d_r}{b} \qquad (6)$$

The rotational speed of the work spindle n can be used to determine the tooth passing frequency T $(= 60/n)$. The gain margin g_m, which is a positive real number that satisfies $\mathrm{imag}(g_m) = 0$, can therefore be determined in a heuristic manner by setting the spindle speed n and the depth of cut d_r as the initial conditions and scanning the chatter vibration frequency ω_c near the natural frequency. A flow chart of the procedure for gain margin analysis is shown in Fig. 2.

Part 1 [6] explained the basic design principles of the anisotropic transfer characteristics for achieving an infinitely large stiffness. As shown in Fig. 3, the pq (modal coordinate system) and xy (process coordinate system) coordinate systems create an angle θ around the z axis. The transfer function ${}^{xy}\boldsymbol{G}(s)$ in the process coordinate system is obtained using Eq. (7).

$$
{}^{xy}\boldsymbol{G}(s) = \begin{bmatrix} G_{xx} & G_{xy} \\ G_{yx} & G_{yy} \end{bmatrix} = \begin{bmatrix} \cos\theta & -\sin\theta \\ \sin\theta & \cos\theta \end{bmatrix}^{-1} \begin{bmatrix} G_{pp} & G_{pq} \\ G_{qp} & G_{pp} \end{bmatrix} \begin{bmatrix} \cos\theta & -\sin\theta \\ \sin\theta & \cos\theta \end{bmatrix} \tag{7}
$$

Equation (8) is obtained when the off-diagonal component of the transfer function ${}^{pq}\boldsymbol{G}(s)$ in the pq coordinate system is assumed to be zero.

$$
\begin{bmatrix} G_{xx} & G_{xy} \\ G_{yx} & G_{yy} \end{bmatrix} = \begin{bmatrix} \cos^2\theta\, G_{pp} + \sin^2\theta\, G_{qq} & -\sin\theta\cos\theta\left(G_{pp} - G_{qq}\right) \\ -\sin\theta\cos\theta\left(G_{pp} - G_{qq}\right) & \sin^2\theta\, G_{pp} + \cos^2\theta\, G_{qq} \end{bmatrix} \tag{8}
$$

In other words, the transfer function ${}^{xy}\boldsymbol{G}(s)$ of the xy coordinate system is composed of the diagonal components G_{pp} and G_{qq} in the pq coordinate system. The weighted linear sum of each component can also be adjusted according to angle θ.

3. Verification of the dynamic characteristics of the prototyped tools with hammering tests

Prototypes of the proposed tools with L/D4 and L/D10 based on the structural design in Part 1 [6] were each fabricated with anisotropic transfer characteristics. A commercially available tool holder for the general-use tool with L/D4 and a newly designed prototyped tool for the general-use tool with L/D10 were compared. Figure 4 shows the CAD model of each tool. A cutting insert made of sintered tungsten carbide and a dummy insert tool were each fixed with a bolt on the free end of the prototyped tool holder. However, only the cutting insert fabricated of sintered tungsten carbide was fixed on the commercially available tool with L/D4. The prototyped tool holder was fixed on a tool holder in the lathe, and the FRF was assessed using impulse excitation tests. The acceleration generated in the xy-axis directions was measured by fixing a small accelerometer on the insert and exciting the tool holder in the direction of the xy-axis. The measurement results are summarized in Table 1. The general-use tool and proposed tool with L/D4 are referred to as I4 and A4, respectively. The general-use tool with L/D10 is referred to as I10, and the proposed tools are referred to as A10-1 and A10-2. Details regarding the shape of each tool and the FEM analysis results are detailed in Part 1 [6]. Details of the measurement results of the frequency response characteristics are shown below, and the FEM analysis results in Part 1 and those obtained here are compared.

3.1 Dynamic characteristics of the prototyped boring tool with L/D4

Figure 5 shows the FRFs of the measured boring tool with L/D4. As shown in Fig. 5 (a), the diagonal components G_{xx} and G_{yy} of the general-use tool (I4) had a similar magnitude. Compared with the diagonal component G_{xx},the off-diagonal component G_{xy} was small at 0.8 μm/N. Meanwhile, as shown in Fig. 5 (b), the compliance ratio $\max(|G_{qq}|) / \max(|G_{pp}|)$ of the proposed tool (A4) was approximately 2.59, and a similar curve was observed in the pq coordinate system. The natural frequency difference $f_{nq} - f_{np}$ was approximately -9.8 Hz. The off-diagonal component G_{pq} in the pq coordinate system was 4.2 μm/N and was not relatively small; however, the diagonal component G_{xx} and off-diagonal component G_{xy} in the xy coordinate system had roughly similar characteristics.

Next, Fig. 6 shows the assessment results of the relationship between the force ratio K_r and chip flow angle η for the maximum negative real part $\max(-\Phi_{re}(i\omega_c))$ of the equivalent transfer function from the measured FRF. The general-use tool (I4) showed tendencies of decreasing maximum negative real part $\max(-\Phi_{re}(i\omega_c))$ and improved stability under the conditions in which the chip flow angle η and force ratio K_r were large. The minimal value of the maximum negative real part $\max(-\Phi_{re}(i\omega_c))$ was 0.59 μm/N when the chip flow angle η was $76°$. The FEM-based analysis results shown in Part 1 also had similar tendencies. However, the FEM analysis showed that the minimal value of the maximum negative real part $\max(-\Phi_{re}(i\omega_c))$ was obtained when the chip flow angle η was $90°$. Thus, even slight differences in the transfer characteristics of the general-use tool affected the equivalent transfer function during the cutting process. The influence of the off-diagonal component G_{xy} was particularly large.

Figure 6 shows that the equivalent transfer function of the proposed tool (A4) has a minimal value at approximately $K_r \cos\eta = 0.5$ which is represented with a white dashed line. The results of FEM analysis shown in Part 1 showed that the maximum negative real part was minimal at approximately $K_r \cos\eta = 0.13$; however, this was due to the different compliance ratio $\max(|G_{qq}|)/\max(|G_{pp}|)$. The tendencies of the chip flow angle η where the maximum negative real part decreased were in line with those of the analysis results related to the influence of the compliance ratio shown in Part 1 when considering the fact that the compliance ratio $\max(|G_{qq}|) / \max(|G_{pp}|)$ was 2.59, as shown in Fig. 5. The minimum value of the maximum negative real part of the proposed tool (A4) decreased by approximately 30% when compared

to that of the general-use tool (I4).

The above assessments showed that the stability of the proposed tool prototype improved by a factor of approximately 3.3 compared to the general-use tool. Furthermore, a smaller maximum negative real part could be obtained at an even smaller chip flow angle when compared to the general-use tool. Therefore, the proposed tool is expected to improve stability not only during rough cutting with large cutting depth, but also in finishing cutting in which the radial depth of cut is small. In other words, the effects of stability improvement that are robust to cutting conditions can be anticipated.

3.2 Dynamic characteristics of the prototyped boring tool with L/D10

Figure 7 shows the measured FRFs for the L/D10 general-use tool (I10) and the proposed tools (A10-1) and (A10-2). The natural frequencies of the diagonal component in the pq coordinate system for each tool matched well. The compliance ratio $\max(|G_{yy}|) / \max(|G_{xx}|)$ in the general-use tool (I10) was 0.65, and some degree of anisotropy was observed. This was thought to be due to the influences of the jig or table structure stiffness. However, the off-diagonal component G_{xy} was small at 6 μm/N, and it was hypothesized that there were virtually no effects of anisotropy with respect to stability. Meanwhile, the designed proposed tools (A10-1) and (A10-2) had compliance ratios $\max(|G_{qq}|) / \max(|G_{pp}|)$ of approximately 1.54 and 1.61, respectively, and roughly similar FRF profiles were obtained. These results mostly matched the results of FEM analysis [6]. Meanwhile, the quality factor Q was larger than the values predicted by the FEM analysis at approximately 150. The off-diagonal components G_{pq} and G_{qp} in the pq coordinate system were also not small at approximately 120–170 μm/N.

Next, the equivalent transfer function $\Phi(i\omega_c)$ was calculated using the measured FRFs. Figure 8 shows the analysis results of the effects of the force ratio K_r and chip flow angle η on the maximum negative real part $\max(-\Phi_{re}(i\omega_c))$ of the equivalent transfer function. The solid white line indicates where $\max(-\Phi_{re}(i\omega_c)) = 20$μm/N. The maximum negative real part of the general-use tool decreased and the stability improved when the K_r and chip flow angle η were large. This trend agreed with those of the FEM analysis-based results [6] of the general-use tool (I10). Meanwhile, the minimum value of the maximum negative real part $\min(\max(-\Phi_{re}(i\omega_c)))$ was approximately 4.5 μm/N and was around 2.5 times more unstable than the FEM-based analysis results. This was thought to be due to the increased

compliance because of the increased Q value compared with the value used for the FEM analysis (Q≒50).

Figure 8 shows that the proposed anisotropic tools (A10-1) and (A10-2) had a minimal equivalent transfer function when $K_r \cdot \cos\eta$ was approximately 0.21 and 0.13, respectively. These trends agreed with those of the FEM-based analysis results [6]. Meanwhile, the minimum values of the maximum negative real part were 8.31 and 10.92 μm/N, respectively, which were larger than those obtained by the FEM analysis [6], which were 0.13 and 1.31 μm/N, respectively; furthermore, it can be seen that the stability was low. This was thought to be due to the decreased similarity of the diagonal component G_{xx} and off-diagonal component G_{xy} because the system developed low damping characteristics [6]. Therefore, it was shown that the effects of the proposed design method would be weaker in long protruding structures with a high Q value. To avoid this, the compliance needed to be decreased, and the similarity between the diagonal component G_{xx} and off-diagonal component G_{xy} needed to be improved by decreasing the Q value. Furthermore, the minimum values of the maximum negative real part of the two proposed tools were larger than those of the general-use tool (I10). In other words, the general-use tool had higher stability when the two most stable conditions were compared. Meanwhile, the two proposed tools could minimize their maximum negative real parts even at small chip flow angles similar to the results obtained for L/D4. Improved stability can be anticipated with the proposed tools unlike with the general-use tool even under finishing cutting, in which the depth of the cut is small.

4. Verification using cutting experiments

Cutting experiments of carbon steel were conducted using the prototyped tools shown in Section 3, and the stability against chatter vibration was assessed. Figure 9 shows the external appearance of the experimental setups. Note that the inner boring is essentially the same as the outer periphery turning; thus, the outer periphery turning, which is easy to measure and evaluate, was adopted for verification. Cutting oil was not used, and dry cutting was performed. In experiment 1, we used the L/D4 tool with a spindle speed of 768 min^{-1} and feed rate of 0.2 mm/rev. In experiment 2, we used the L/D10 tool with a spindle speed of 390 min^{-1} and feed rate of 0.1 mm/rev. An accelerometer was attached on the back side of the tool, vibrations during machining were measured, and the stability was determined. Furthermore, the results of stability limit analysis shown in Section 2 were implemented and compared with the experimental results. The primary cutting conditions and the identified parameters are shown in Table 2. The specific cutting

force K_t and force ratio K_r in particular were identified by conducting cutting experiments with no vibration using systems with sufficiently high stiffness and by measuring the cutting force.

4.1 Results of the L/D4 cutting experiments

Comparisons of the experimental results and the analysis results in Experiment 1 are shown in Fig. 10. The gain margin g_m was determined directly using the measured FRFs determined in Section 3, which were based on the stability limit analysis methods shown in Section 2. The results shown here considered conditions where the transverse axis was set as the spindle speed n, and the longitudinal axis was set as the depth of cut d_r or the chip flow angle η. Using these results, the $g_m < 1$ range was unstable, the $g_m > 1$ range was stable, and the stability limit $g_m = 1$ was shown using a solid line. Furthermore, the vibration displacement component was analyzed from the acceleration signal measured during experimental machining, and cases in which the amplitude of the vibration displacement component, which is asynchronous with the spindle rotation, was 1 μm or higher were interpreted as the occurrence of chatter vibration and marked with an x. All other cases were interpreted as stable conditions and marked with an o.

The stability range of the general-use tool (I4) was extremely small, with analysis results showing that stability was obtained only in the range where the depth of cut d_r was less than 0.05 mm. Meanwhile, the results of analysis of the proposed tool (A4) showed that stability was observed in the range where the depth of cut d_r was less than 0.08 mm, as well as between 0.5 to 0.85 mm. The stability range was expanded, with the maximum stable depth of the cut limit being approximately 17 times higher than that of the general-use tool (I4). Similar trends were observed in the experimental results based on each tool, and these results showed that the stability improved with the proposed methods. Analysis results of the proposed tool (A4) showed that the stable range with a larger depth of cut d_r corresponded to a chip flow angle η of $43°$ to $60°$. The values of $K_r \cos\eta$ in this range were 0.46 to 0.67. Figure 6 shows that the compliance of the equivalent transfer function for the proposed tool (A4) was minimal at approximately $K_r \cos\eta = 0.5$. Therefore, the stability was thought to have improved under the conditions in that vicinity, and the tendencies agreed with the analysis results of the maximum real negative part of the equivalent transfer function.

Fig. 11 shows a photograph of the external appearance of the finished surface after cutting and the

frequency analysis results of the acceleration measured during cutting. The figure confirmed that chatter vibration occurred in the general-use tool (I4) even under conditions where the depth of the cut was small ($d_r = 0.1$ mm), and clear chatter marks were observed. Microscale chatter vibration occurred because the proposed tool (A4) was unstable under the same conditions where the depth of the cut was small ($d_r = 0.1$ mm). Meanwhile, no chatter vibration occurred under stable conditions where the depth of the cut was large (0.7 mm). The above results confirmed the improved stability of chatter vibration and high-efficiency machining due to the proposed tool.

Next, the influence of the force ratio K_r on chatter stability was analyzed. The force ratio can vary according to the workpiece and tool materials as well as the tool properties. Based on these characteristics, the relationship between the force ratio and chatter stability was important information when considering the practical applications of the proposed method. Figure 12 shows the results of the stability analysis based on the FRF of the prototyped tool, where the spindle speed n was 768 min^{-1}. The boundary where the gain margin g_m is 1 is represented with a black solid line, and $K_r \cos\eta = 0.5$ is demonstrated with a white dashed line. This figure shows the results when the gain margin g_m was analyzed in the range of depth of cut d_r=0 – 1 mm. The figure shows that the stabilization of the general-use tool (I4) occurred only in the $d_r < 0.05$ range when $0.5 \leq K_r$. Meanwhile, stabilization in the proposed tool (A4) occurred in the $d_r < 0.1$ range when $0.5 \leq K_r$ and also near $K_r \cos\eta = 0.55$.

The ratio of gain margins $g_{m,A4}/g_{m,I4}$, where $g_{m,I4}$ and $g_{m,A4}$ were defined as the gain margins of the general-use tool (I4) and the proposed tool (A4), respectively, is shown in Fig. 13. The boundary where the gain margin ratio $g_{m,A4}/g_{m,I4}$ is 1 is represented with a black solid line, and $g_{m,A4}/g_{m,I4} > 1$ signified that the stability of the proposed tool (A4) was higher than that of the general-use tool (I4). The figure shows that the gain margin ratio $g_{m,A4}/g_{m,I4}$ was particularly large in the wide range near $K_r \cos\eta = 0.5$. Thus, the stability of the proposed anisotropic tool (A4) was high, and the value of max $(g_{m,A4}/g_{m,I4})$ improved by a factor of 3.7 under the conditions with maximal differences. From the above results, stability-improving performance was confirmed according to the theory by setting up conditions to satisfy the appropriate $K_r \cos\eta$ according to the compliance ratio. Therefore, the force ratio K_r of the workpiece actually used was determined, and anisotropic tools with compliance ratios that agreed with this force ratio could be selected to achieve cutting with high stability efficiency.

4.2 L/D10 assessment results

Verification experiments were conducted using the general-use tool (I10) and proposed tool (A10-1). Only stability analysis was conducted for the proposed tool (A10-2). Figure 14 shows the comparisons between the experimental results and analysis results of each tool. Cases in which the amplitude of the vibration displacement component, which is asynchronous with the spindle rotation, was 1 μm or higher were interpreted as the occurrence of chatter vibration and marked with an x. As shown in the figure, the gain margin g_m in each tool was less than 1, and a stable range was not achieved. Figure 15 shows the finished surface obtained from the cutting tests. The finished surface obtained by the proposed tools was favorable compared with that obtained using the general-use tools; however, chatter vibration was not controlled. It can be seen from the above results that the stability somewhat improved with the proposed methods, but the effects were insufficient.

Next, the influence of the force ratio on chatter stability was analyzed. Figure 16 shows the analytical results of the gain margin g_m of the general-use tool (I10) and the proposed tools (A10-1) and (A10-2) based on the measurement results of the FRF. As shown in the analysis results in Fig. 14, the stability somewhat varied with the spindle speed. Therefore, a spindle speed for which a comparatively wide stable range can be obtained was selected for each tool, and analyses were conducted with a spindle speed n of 386, 392, and 393 min^{-1}. Stability slightly improved for the general-use tool (I10) when the depth of cut d_r was extremely small or when both the depth of cut d_r and force ratio K_r were large but the overall gain margin g_m was small. Meanwhile, the gain margin g_m of the proposed tool (A10-1) tended to increase in the range near $K_r \cos\eta = 0.22$. This agrees with the tendencies seen in Fig. 8. The increasing tendencies of the gain margin g_m in the same region can be confirmed using the proposed tool (A10-2), but the improvement was not as pronounced as that for the proposed tool (A10-1). Furthermore, the gain margin g_m of both tools was less than 1, and no stable conditions were met.

Figure 17 then shows the gain margin ratios $g_{m,A10-1}/g_{m,I10}$ and $g_{m,A10-2}/g_{m,I10}$ between the proposed tools and general-use tool. The boundary where the gain margin ratio is equal to 1 is shown as a solid black line in the figure. The proposed tool (A10-1) had higher stability than the general-use tool (I10) in the range of $0.19 < K_r \cos\eta < 0.32$. Similar trends were observed for the proposed tool (A10-2), but these were not as pronounced as those observed for proposed tool (A10-1). This agreed with the tendencies of the analysis results of the maximum negative real part shown in Fig. 8. The maximum gain margin ratio

of the proposed tool (A10-1) was max ($g_{m,A10-1}/g_{m,I10}$)=1.8. Here, we consider the experimental results shown in Fig. 15. The experimental depth of the cut d_r was 0.5 mm, and the force ratios were $K_r = 0.610$ (I10) and $K_r = 0.527$ (A10-1). $g_{m,A10-1}/g_{m,I10} = 1.07$ under these conditions, and the proposed tool showed a somewhat higher stability. Thus, the finished surface obtained by experiments showed somewhat improved stability.

Based on the above results, chatter stability slightly improved with the proposed methods, but stable conditions were not achieved with the proposed L/D10 tool prototype. Thus, analytical investigations were conducted using the proposed tool (A10-1) to understand the mechanisms by which transfer characteristics could be improved to achieve stable conditions. First, the modal parameters ω_n, ζ, and k in the direction of the pq-axis were calculated from the FRFs determined from the impulse response tests. However, the influence of the off-diagonal component was ignored by forcing it to zero. Next, the influence of each parameter was analyzed by revising each of these parameters and performing stability analysis. Analyses were conducted here using a spindle speed of n=392 min^{-1}. The design values of the modal parameters are shown in Table 3. The parameters in Condition 1 were those identified from the measured FRF and were set as the standard condition. The standard conditions were used for Condition 2, with the exception of the natural frequency difference $f_q - f_p$, which was changed to zero. The standard conditions were used for Condition 3, with the exception of Q_p which was changed to Q_q. The compliance $\max(|G_p|)$ was set to a tenth of the value in the standard condition for Condition 4. Condition 5 involved all the revisions made in Conditions 2–4.

Figure 18 shows the influence of the force ratio and cutting on the gain margin for each condition. The range of the color bar was set to $0 \leq g_m \leq 0.1$ in Fig. 18 (a) – (c), and $0 \leq g_m \leq 2$ in Fig. 18 (d) and (e). Furthermore, the boundary at which the gain margin $g_m = 1$ is represented with a black solid line. Stability somewhat improved at approximately $K_r \cos\eta = 0.4$ for the standard conditions (Condition 1), but $g_m < 1$ for the entire range, and the analysis results showed instability. The $K_r \cos\eta$ distribution where stability improved was slightly different when compared with the gain margin calculated using the experimentally measured data including the off-diagonal components of the same FRF (Fig. 16 (b)). This was thought to be because the off-diagonal components G_{pq} and G_{qp} were ignored in the analysis in Fig. 18.

The analysis results of Conditions 2 and 3 showed that revising the natural frequency difference $f_q - f_p$ and Q_q/Q_p was not effective in increasing the gain margin. However, the $K_r \cos\eta$ range that improved the stability changed relative to that seen in Condition 1. This suggests that the natural frequency difference $f_q - f_p$ and the damping ratio error ζ_q/ζ_p influenced the optimal conditions of $K_r \cos\eta$. The analysis results of Condition 4 in Fig. 18 (d) show that reductions in the compliance $\max(|G_p|)$ had a large effect. Condition 5 showed that a stable range was achieved across an even wider set of conditions. A high stability was shown to be possible in this way by simultaneously reducing the compliance and revising the natural frequency and Q value differences.

The maximum gain margin value was $\max(g_m) = 0.21$ under the range of the depth of cut above 0.2 mm for the standard condition (Condition 1). Meanwhile, a stable range where $g_m \geq 1$ was observed across a wide range for Condition 5 and stable effects which were robust against cutting conditions changes are anticipated. The above results confirmed that a stable range for the L/D10 tool could be achieved by improving the concordance rate of the natural frequency error and Q value in the pq-axis and by decreasing the maximum compliance value $\max(|G_p|)$. However, adjusting the transfer characteristics to this level of accuracy in practice is not a simple task. Therefore, novel techniques that can adjust the dynamic stiffness to an even higher accuracy are needed to achieve the proposed techniques for structures above L/D10.

5. Conclusions

A novel boring tool that suppresses chatter vibration using an anisotropic structure was prototyped, and practical applications to turning operations were confirmed using verification experiments. For the proposed method, the anisotropy associated with the boring tool was used to improve the dynamic stiffness during the cutting process. In this study, we tested three L/D4 and L/D10 tool holders that were designed using the FEM analyses in Part 1, and the effects of the proposed methods were analyzed through verification experiments. Furthermore, issues related to practical applications were investigated. The conclusions obtained are summarized as follows:

1. Analysis results of the FRF of the proposed L/D4 tool prototype showed that the desired anisotropic transfer characteristics were mostly achieved, and theoretical improvements to stability relative to that in the general-use tool could be expected. Improvements in stability were also achieved in the cutting experiments, with the stable depth of the cut limit improving by a factor of approximately

17 relative to that of the general-use tool.

2. Analysis results of the FRF of the proposed L/D10 tool prototype showed that the quality factor Q was approximately three times larger than that in the FEM analysis results, and that no large stability effects were anticipated. Cutting experiments also showed some degree of stability improvement relative to that in the general-use tool, but chatter vibration could not be avoided.
3. Compliance needed to be further decreased to achieve the desired stability range in the proposed L/D10 tool. Adjustments to further match the natural frequency and Q value between modes were effective in improving stability. Practical methods that can accurately control stiffness are needed to achieve this purpose.

Acknowledgments

The Authors thank Mr. Watanabe and Mr. Nishigata. They made enormous contirbutions in the early stages of research.

Funding sources

This work was partially suppourted by JSPS KAKENHI Grant Number 22760097.

References

[1] Altintas Y. Manufacturing automation 2nd edition, Cambridge University Press, 2012

[2] Andrén L, Håkansson L, Brandt A, Claesson I. Identification of motion of cutting tool vibration in a continuous boring operation—correlation to structural properties. Mech Syst Signal Proces 2004;18(4):903–27.

[3] Eynian M, Altintas Y. Chatter stability of general turning operations with process damping. J Manuf Sci Eng 2009;131(4).

[4] Shamoto E, Fujimaki S, Sencer B, Suzuki N, Kato T, Hino R. A novel tool path/posture optimization concept to avoid chatter vibration in machining–proposed concept and its verification in turning. CIRP Annals 2012;61(1):331–4.

[5] Suzuki N, Nishimura K, Watanabe R, Kato T, Shamoto E. Development of novel anisotropic boring tool for chatter suppression. Procedia CIRP 2012;1:56–9.

[6] Takahashi W, Suzuki N, Shamoto E. Development of a novel boring tool with anisotropic dynamic stiffness to avoid chatter vibration in cutting Part 1: design of anisotropic structure to attain infinite dynamic stiffness. Precision Engineering, in press

Figure Captions

Fig. 1 Block diagram of the boring process with chatter vibration.

Fig. 2 Flowchart of the gain margin calculation for chatter stability analysis.

Fig. 3 Relative relationship between the xy coordinate system and pq coordinate system.

Fig. 4 Proposed and conventional boring tools.

Fig. 5 FRFs of the prototyped L/D4 boring tools measured by hammering tests.

Fig. 6 Influence of the force ratio and chip flow angle on the maximum of the negative real part of equivalent transfer function (L/D4). (Measured FRFs in Fig. 5 are used)

Fig. 7 FRFs of the prototyped L/D10 boring tools measured by hammering tests.

Fig. 8 Influence of the force ratio and chip flow angle on the maximum of the negative real part of equivalent transfer function (L/D10). (Measured FRFs in Fig. 7 are used)

Fig. 9 Experimental setup for the peripheral turning tests using the developed boring tools.

Fig. 10 Stability limit diagram for L/D4 tools (Analysis: color map, Experiment: plots)
(i) Influence of depth of cut, (ii) Influence of chip flow angle.

Fig. 11 Frequency analysis result of the acceleration measurement and finished surface after cutting (L/D4)

Fig. 12 Influence of depth of cut and force ratio on gain margin (L/D4). (Measured FRFs in Fig. 5 are used)

Fig. 13 Gain margin improvement ratio of model (A4) to model (I4). (Measured FRFs in Fig. 5 are used)

Fig. 14 Stability limit diagram for the L/D10 tools (Analysis: color map, Experiment: plots)
(i) Effect of the depth of cut (ii) Effect of the chip flow angle.

Fig. 15 Finished surface after cutting (L/D10, d_r= 0.50 mm).

Fig. 16 Influence of depth of cut and force ratio on gain margin (L/D10). (Measured FRFs in Fig.7 are used)
(a) I10, 386min^{-1} (b) A10-1, 392min^{-1} (c) A10-2, 393min^{-1}

Fig. 17 Gain margin improvement ratio of model (A10) to model (I10). (Measured FRFs in Fig. 7 are used)

Fig. 18 Stable limit region after parameter adjustment in model (A10-1) (Modal parameters in Table 3 are used) (L/D10, n=392min^{-1}).

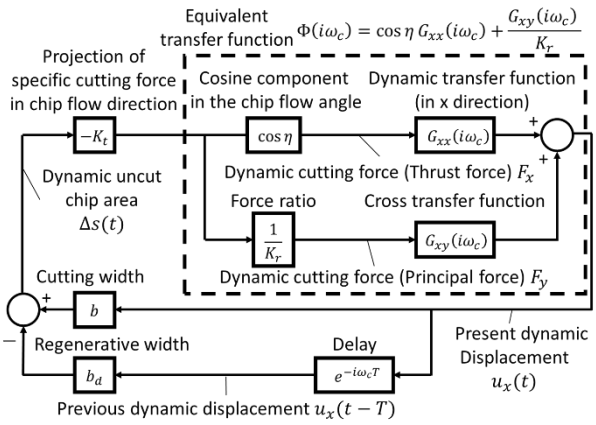

Fig. 1 Block diagram of the boring process with chatter vibration.

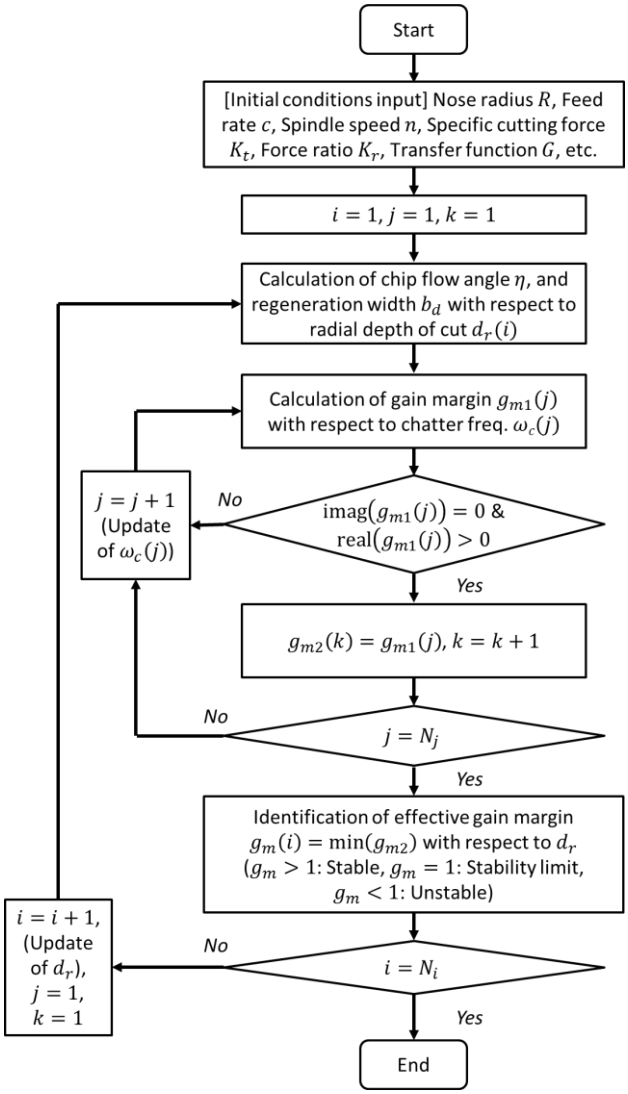

Fig. 2 Flowchart of the gain margin calculation for chatter stability analysis.

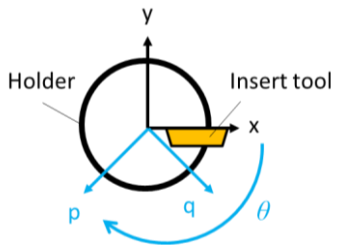

Fig. 3 Relative relationship between the xy coordinate system and pq coordinate system.

(a) General-use conventional L/D4 tool (I4)

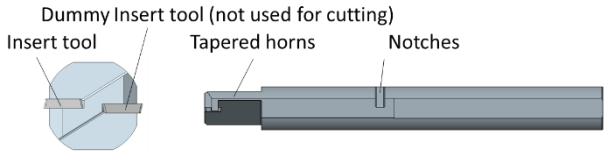

(b) Prototype of proposed L/D4 tool (A4)

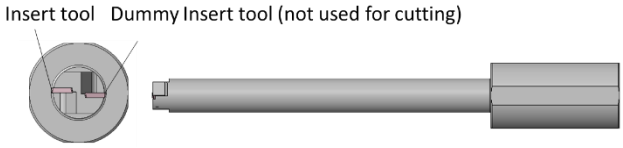

(c) Prototype of conventional L/D4 tool (I10)

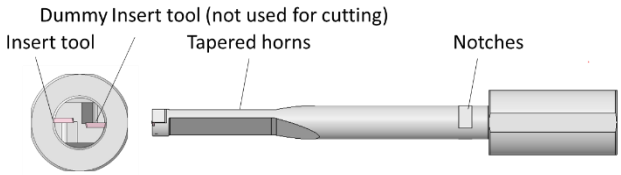

(d) Prototype of proposed L/D10 tool (A10-1)

Fig. 4 Proposed and conventional boring tools.

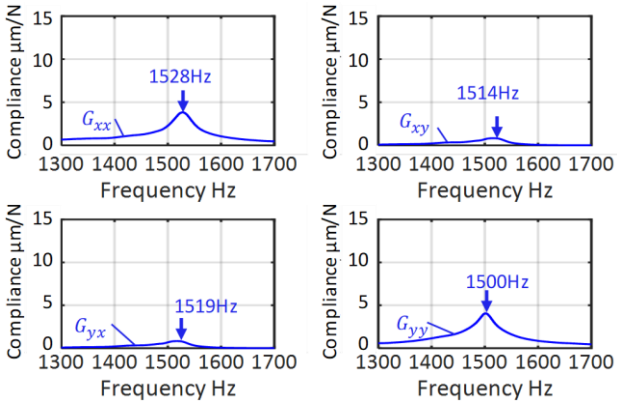

(a) I4 (Conventional)

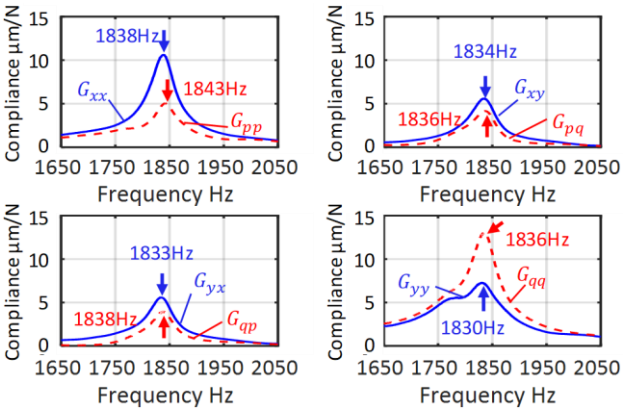

(b) A4 (Proposed)

Fig. 5 FRFs of the prototyped L/D4 boring tools measured by hammering tests.

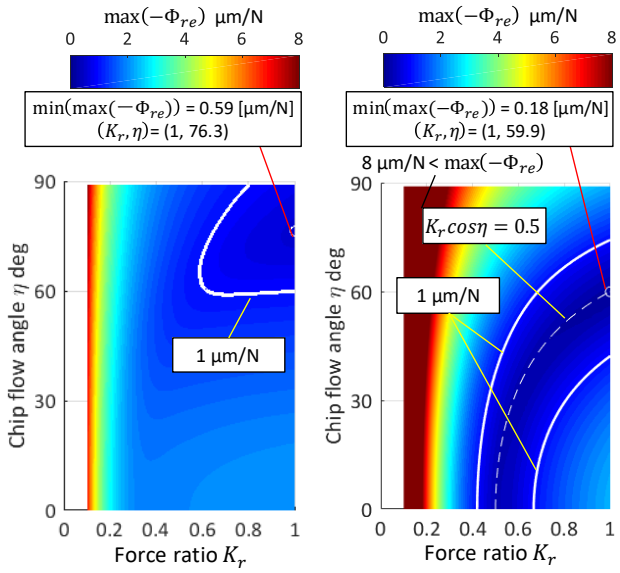

(a) I4 (Conventional) (b) A4 (Proposed)

Fig. 6 Influence of the force ratio and chip flow angle on the maximum of the negative real part of equivalent transfer function (L/D4).

(Measured FRFs in Fig. 5 are used)

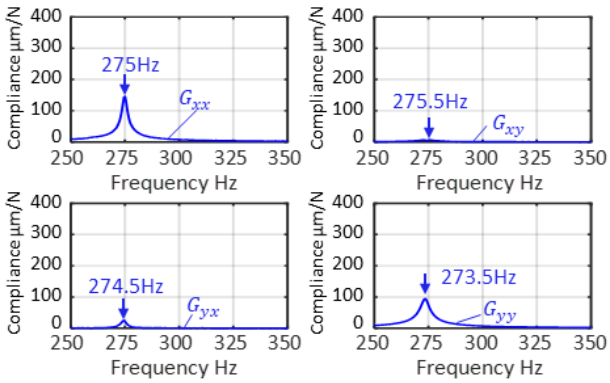

(a) I10 (Conventional)

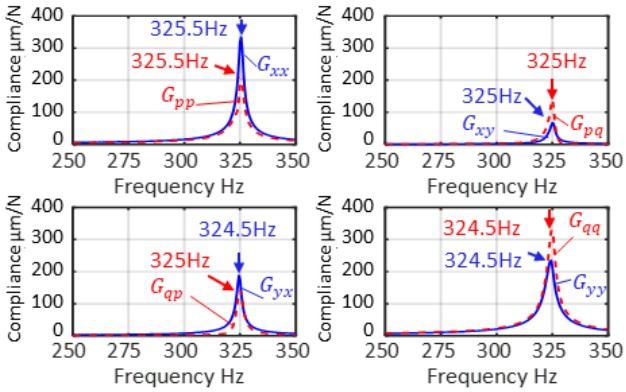

(b) A10-1 (Proposed)

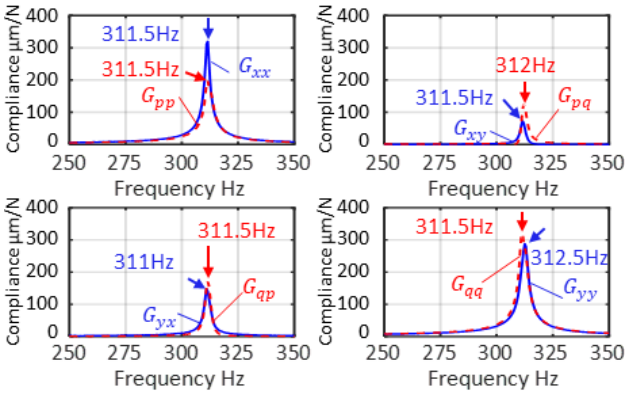

(c) A10-2 (Proposed)

Fig. 7 FRFs of the prototyped L/D10 boring tools measured by hammering tests.

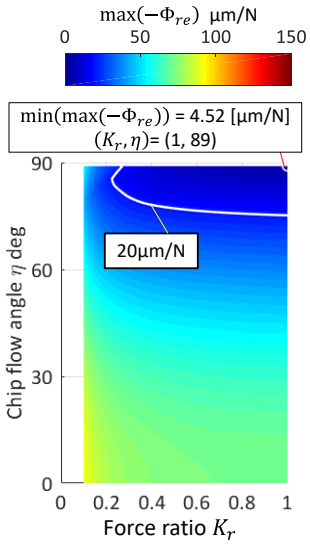

(a) I10 (Conventional)

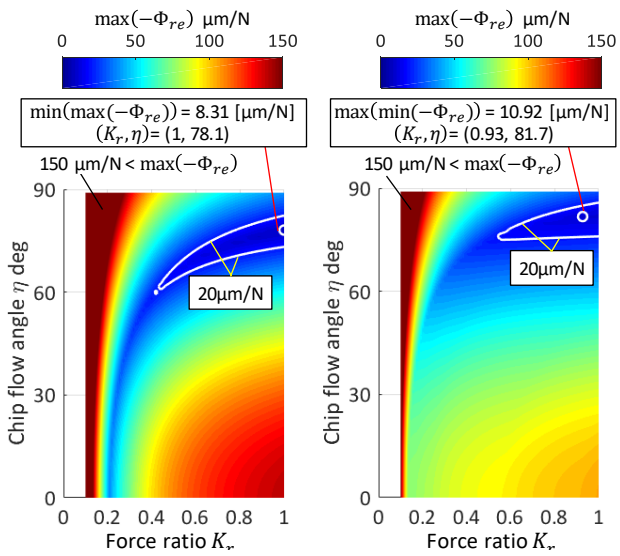

(b) A10-1 (Proposed) (c) A10-2 (Proposed)

Fig. 8 Influence of the force ratio and chip flow angle on the maximum of the negative real part of equivalent transfer function (L/D10).

(Measured FRFs in Fig. 7 are used)

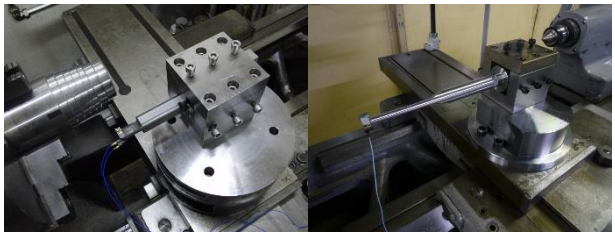

(a) L/D4 (b) L/D10

Fig. 9 Experimental setup for the peripheral turning tests using the developed boring tools.

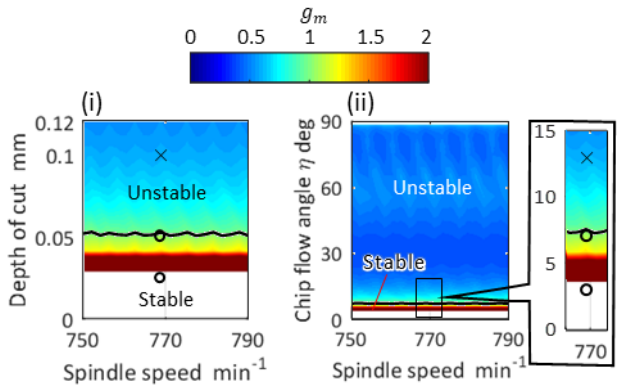

(a) I4 (Conventional)

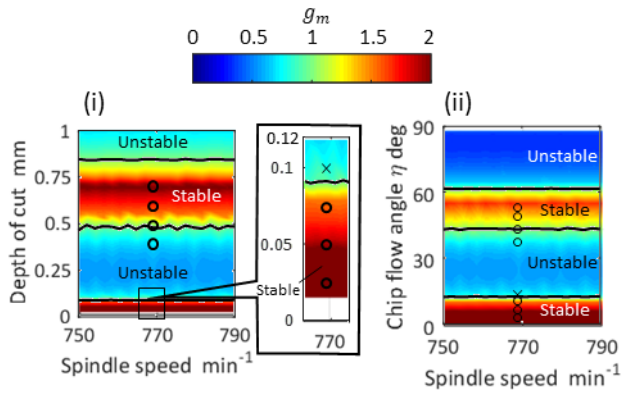

(b) A4 (Proposed)

Fig. 10 Stability limit diagram for L/D4 tools (Analysis : color map, Experiment : plots)

(i) Influence of depth of cut (ii) Influence of chip flow angle.

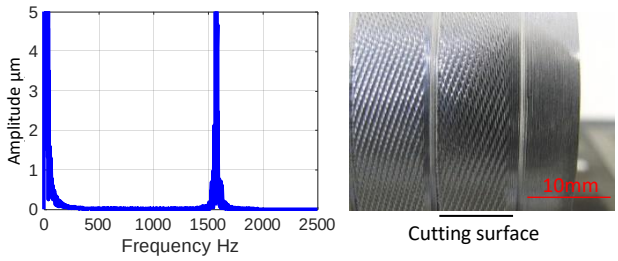

(a) d_r= 0.10 mm, I4 (Conventional)

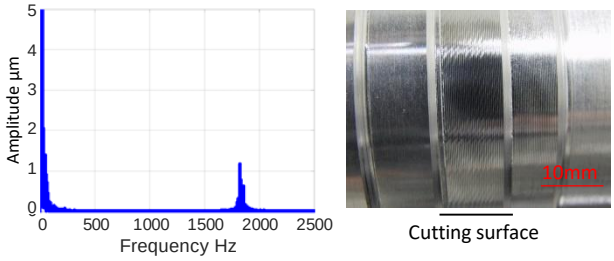

(b) d_r= 0.10 mm, A4 (Proposed)

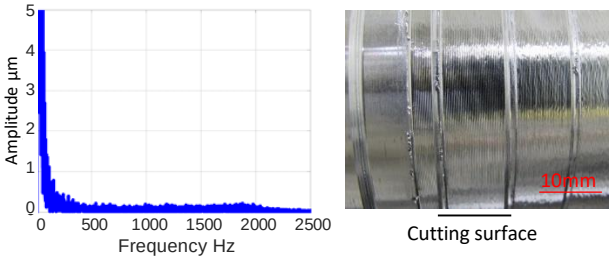

(c) d_r= 0.70 mm, A4 (Proposed)

Fig. 11 Frequency analysis result of the acceleration measurement and finished surface after cutting (L/D4).

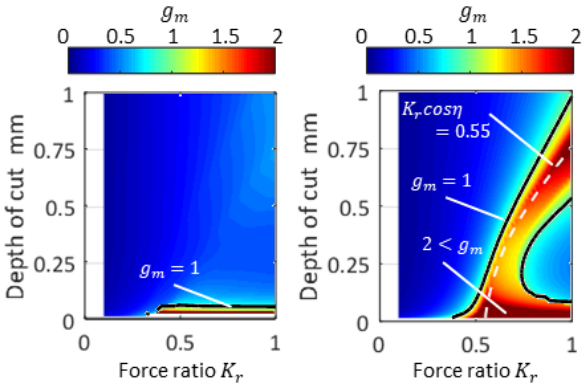

(a) I4 (Conventional) (b) A4 (Proposed)

Fig. 12 Influence of depth of cut and force ratio on gain margin (L/D4) (Measured FRFs in Fig. 5 are used).

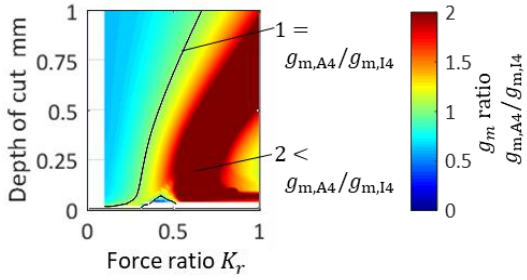

Fig. 13 Gain margin improvement ratio of model (A4) to model (I4).

(Measured FRFs in Fig. 5 are used)

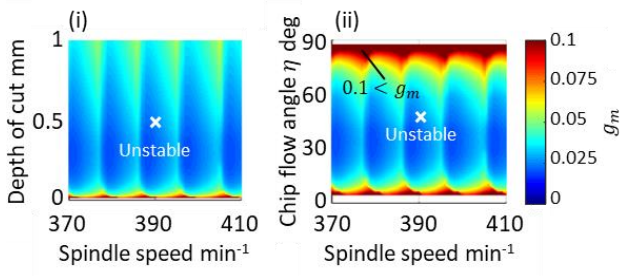

(a) I10 (Conventional)

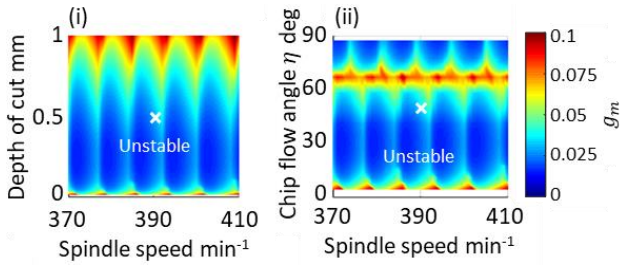

(b) A10-1 (Proposed)

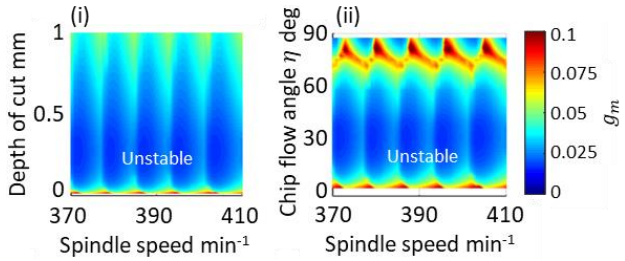

(c) A10-2 (Proposed)

Fig. 14 Stability limit diagram for the L/D10 tools (Analysis: color map, Experiment: plots)

(i) Effect of the depth of cut (ii) Effect of the chip flow angle.

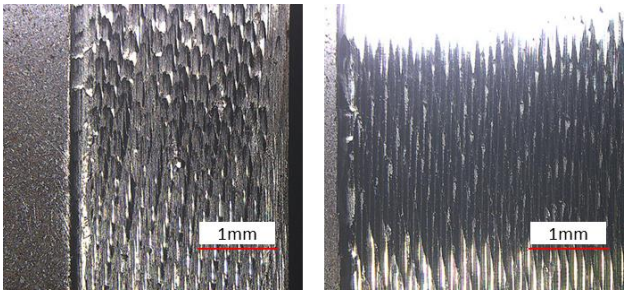

(a) I10 (Conventional) (b) A10-1 (Proposed)

Fig. 15 Finished surface after cutting (L/D10, d_r= 0.50 mm).

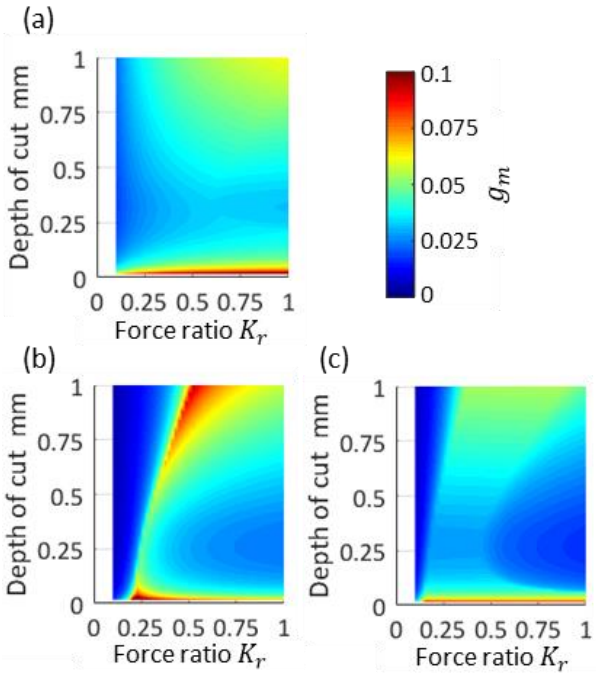

Fig. 16 Influence of depth of cut and force ratio on gain margin (L/D10) (Measured FRFs in Fig.7 are used).

(a) I10, 386min^{-1} (b) A10-1, 392min^{-1} (c) A10-2, 393min^{-1}

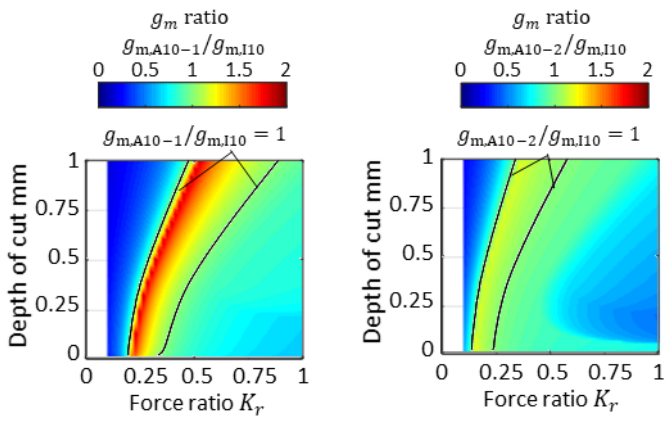

(a) A10-1 (Proposed) (b) A10-2 (Proposed)

Fig. 17 Gain margin improvement ratio of model (A10) to model (I10).

(Measured FRFs in Fig. 7 are used)

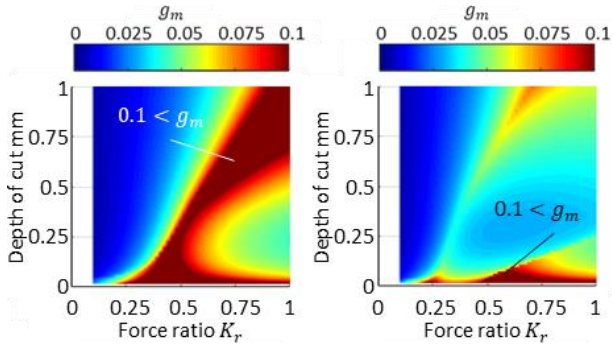

(a) Cond. 1

(b) Cond. 2

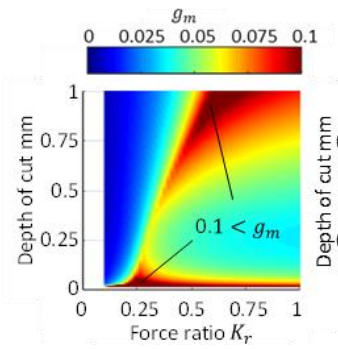

(c) Cond. 3

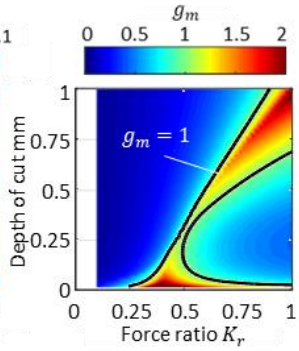

(d) Cond. 4

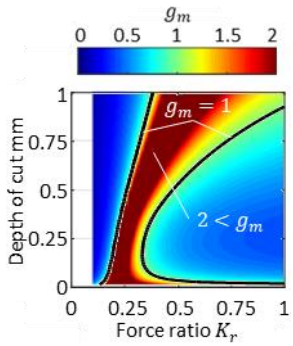

(e) Cond. 5

Fig. 18 Stable limit region after parameter adjustment in model (A10-1).

(Modal parameters in Table 3 are used) (L/D10, 392min^{-1})

Table 1 Experimental results (L/D4,10)

Model	Q	Natural frequency in p axis f_{np} Hz	Maximum compliance in p axis $\max(\lvert G_{pp} \rvert)$ μm/N	Natural frequency difference $f_{nq} - f_{np}$ Hz	Compliance ratio $\frac{\max(\lvert G_{qq} \rvert)}{\max(\lvert G_{pp} \rvert)}$
I4	39	1523	3.9	-24.5	1
A4	46	1842	5	-9.8	2.59
I10	113	275	145.7	-1.4	0.65
A10-1	168	325.5	213.5	-0.8	1.54
A10-2	153	312	198.5	-0.1	1.61

Table 2 Experimental conditions and identified parameters

		Exp. 1 (L/D4)	Exp. 2 (L/D10)
Workpiece material		SS400, ϕ65 ~ 80	
Specific cutting force K_t	GPa	2.27	1.25 (I10) 1.2 (A10-1)
Cutting force ratio K_r		0.914	0.610 (I10) 0.527 (A10-1)
Nose radius R	mm	0.4	
Approach angle	deg	-1	0
Wedge angle	deg	60	
Spindle speed	min^{-1}	768	390
Cutting speed	m/min	150～200	104
Feed rate	mm/rev	0.2	0.1

Table 3 Parameters used for stability analyses

Condition	f_p Hz	$f_q - f_p$ Hz	Q_p	$\frac{Q_q}{Q_p}$	$\max(\lvert G_p \rvert)$ μm/N	$\frac{\max(\lvert G_q \rvert)}{\max(\lvert G_p \rvert)}$
1 (reference)	325.5	-1	168	0.58	213.5	1.54
2		**0**				
3		-1		**1**		
4				0.58	**21.4**	
5		**0**		**1**		